ENVIRONMENTAL RESEARCH
CLIMATE

OPEN ACCESS

RECEIVED
5 July 2024

REVISED
21 November 2024

ACCEPTED FOR PUBLICATION
6 December 2024

PUBLISHED
27 December 2024

PAPER

Sea ice perturbations in aquaplanet simulations: isolating the physical climate responses from model interventions

M R England[1,2,*], **N Feldl**[2] **and I Eisenman**[3]

[1] Department of Mathematics and Statistics, University of Exeter, Exeter, United Kingdom
[2] Department of Earth and Planetary Sciences, University of California Santa Cruz, Santa Cruz, CA, United States of America
[3] Scripps Institution of Oceanography, University of California San Diego, La Jolla, CA, United States of America
[*] Author to whom any correspondence should be addressed.

E-mail: m.england2@exeter.ac.uk

Keywords: sea ice, aquaplanet, climate model, model hierarchy, polar climate change, slab ocean

Supplementary material for this article is available online

Abstract

Comprehensive climate model simulations with perturbed sea ice covers have been extensively used to assess the impact of future sea ice loss, suggesting substantial climate changes both in the high latitudes and beyond. However, previous work using an idealized energy balance model calls into question the methods that are used to perturb sea ice cover, demonstrating a consistent overestimate of the surface warming due to sea ice loss, while the large complexity gap between the idealized and comprehensive models makes the implications of this result unclear. To bridge this gap we have performed simulations with a new implementation of the CESM2 model in a slab ocean aquaplanet configuration coupled with thermodynamic sea ice, which is able to capture the realistic seasonal characteristics of polar climate change. Using this model setup, we perform a suite of experiments to systematically quantify the spurious climate responses associated with melting sea ice without a CO_2 forcing. We find that using the sea ice ghost flux method overestimates many aspects of the climate response by 10%–20%, including the polar warming, the mini global warming signal and the increase in both precipitation and evaporation. The location of the latitudinal band of heating applied to melt the sea ice relative to the midlatitude jet is important for determining where the midlatitude circulation response is overestimated. This work advances our ability to isolate the true climate response to sea ice loss, and provides a framework for conducting coupled sea ice loss simulations absent the spurious impacts from the addition of artificial heating.

1. Introduction

Results from coupled sea ice loss simulations suggest polar sea ice loss has wide ranging impacts on the rest of the climate system. These include surface-dominated polar amplified warming (e.g. Deser *et al* 2015, Screen *et al* 2018), an equatorward shift or a weakening of the poleward flank of the midlatitude tropospheric jet (e.g. Blackport and Kushner 2017, Screen *et al* 2018, Simon *et al* 2021, Ayres *et al* 2022), a weakening of the Atlantic Meridional Overturning Circulation (Sevellec *et al* 2017), an intensification of the equatorward flank of the ITCZ (e.g. England *et al* 2020), a warming of the tropical upper troposphere (e.g. Deser *et al* 2015, Screen *et al* 2018, England *et al* 2020) and even a response at the opposite pole (England *et al* Sun 2020, Ayres *et al* 2022). These studies typically compare a control simulation with a perturbed sea ice simulation, which is identically forced except that the sea ice cover is artificially constrained to match a reduced future sea ice state, and they focus on the equilibrium response through performing repeated time-slice experiments.

There is no agreed-upon best practice for constraining sea ice cover in coupled simulations, so these modelling studies rely on a variety of different methods to achieve the diminished sea ice cover without increasing CO_2 concentration. The methods for melting the sea ice include adding a longwave flux to the sea ice model, known as the ghost flux method (e.g. Deser *et al* 2015), modifying the albedo parameters of the

sea ice model to reflect less incoming shortwave radiation (e.g. Blackport and Kushner 2017), and directly nudging the sea ice cover by simply removing sea ice (e.g. Peings *et al* 2021). However, the study of England *et al* (2022), hereafter referred to as EEW22, demonstrated in an idealized model of sea ice and climate that these widely used methods for perturbing sea ice cover in coupled simulations may be overestimating the surface warming attributable to ice loss. In fact, that study found that the overestimation is of considerable magnitude: surface warming in response to sea ice loss was exaggerated in this idealized model by a factor of 1.5–2.0. The recent study of Fraser-Leach *et al* (2023) attempt to quantify and remove the spurious effects of the albedo modification method from comprehensive climate model simulations using a statistical-based pattern scaling approach, and find a similar factor of 1.5–2.0.

Why do these methods overestimate the surface warming in response to sea ice loss? EEW22 argue that an artificial heating applied in the high latitudes to melt the sea ice is used to achieve the intended loss of sea ice. This artificial heating will then generate a climate response of its own, and this is being spuriously attributed to the role of sea ice loss. For the ghost flux method it is unambiguous that additional heat is explicitly being inserted into the high latitudes. For the case of direct nudging through removing sea ice, this will require a net input of latent heat. Although the modification of sea ice albedo parameters conserves energy, the surface of the high latitudes is artificially heated because the remaining sea ice cover will reflect less incoming shortwave radiation than in the greenhouse-forced warming simulation. In other words, the change in surface albedo required to melt the sea ice is larger than the albedo change directly associated with the sea ice loss. We note that Sun *et al* (2020) find that simulations using albedo modification and nudging produce very similar estimates for the effects of sea ice loss. The implication of the results of EEW22 is that the climate response to sea ice loss may be overestimated in coupled climate model simulations, whichever standard method is used to perturb the sea ice cover.

However, EEW22 has three major limitations which make it challenging to interpret the results in the context of existing comprehensive climate model simulations. Firstly, the energy balance model used in EEW22 is highly idealized and lacks representation of many important processes in the real climate system which would be simulated by comprehensive climate models, such as clouds, an atmospheric circulation, atmospheric moisture, and ocean dynamics. Hence, it is important to understand how these missing processes could modulate the spurious response to artificial heating in a more complex climate model. Secondly, the analysis of the spurious climate response in EEW22 is restricted to examining surface temperature and sea ice thickness because these are the only state variables in the energy balance model, and so the response, for instance, of precipitation or the midlatitude jet is challenging to infer. Therefore, a logical next step is to utilise a climate model able to directly simulate these features of the atmospheric response. Lastly, EEW22 did not explicitly propose a framework for removing the spurious climate response from existing comprehensive model simulations, or offer an alternative approach absent these methodological artefacts. In this study we aim to address all three of these previous limitations by performing and analysing simulations with a climate model much further up the complexity hierarchy which well simulates the relevant features of the climate system. Using this model setup, we will outline a framework for accounting for the spurious effects of model intervention and providing an improved estimate of the actual role of sea ice loss.

2. CESM2 slab ocean aquaplanet with thermodynamic sea ice

In this study, we employ the slab ocean aquaplanet configuration of the Community Earth System Model Version 2 (CESM2-CAM6) (Danabasoglu *et al* 2020), identical to that used by the recent study of England and Feldl (2024) which investigated polar amplification in ice-free climates, except coupled to a thermodynamic representation of sea ice. In brief, the atmospheric component, the Community Atmosphere Model Version 6, is run with a horizontal resolution of 1.9° by 2.5° and 32 vertical levels and is coupled to a slab ocean of 30 m mixed layer depth. We prescribe an annual-mean semi-idealised q-flux profile averaged from 500 years of the CESM2-CAM6 $4\times CO_2$ simulation. For further details on this imposed ocean heat transport, please refer to section 2b3 and figures 2(c) and S1(c) of England and Feldl (2024). Our setup includes the full seasonal cycle (obliquity of 23.45° and eccentricity of 0). We employ the Last Glacial Maximum constrained version of CESM2-CAM6 through minor alterations to the cloud microphysics and ice nucleation code, which leads to a substantially lower climate sensitivity than the default version (Zhu *et al* 2022). The aerosol emissions and ozone concentrations, taken from the CESM2-CAM6 1850 pre-industrial control simulation, are zonally-averaged and symmetrised about the equator, so as not to introduce any hemispheric or zonal asymmetries into our simulations.

The only difference with the model configuration of England and Feldl (2024) is that here, instead of neglecting sea ice, we couple the atmosphere and slab ocean to an idealised representation of thermodynamic sea ice. For the sea ice CICE model, the thermodynamics is governed by the zero-layer model of Semtner (1976), in a similar fashion to the implementation of Chung and Feldl (2024). This model has only two

prognostic variables—snow thickness and ice thickness—with an assumed linear profile of interior temperature. Given its simplicity, this model surprisingly captures the main characteristics of ice thickness as simulated by more complex schemes (see appendix of Semtner (1976)), especially for the case of the annual mean thickness. The thermal conductivity of snow and sea ice are set to 0.3 $Wm^{-1}K^{-1}$ and 2.0 $Wm^{-1}K^{-1}$ respectively (Semtner 1976). We note that the stability of the polar sea ice caps in this slab ocean configuration of CESM2-CAM6 including a zero-layer thermodynamic ice model is particularly sensitive to the prescribed latitudinal profile of the q-flux. More specifically, consistent with previous studies (e.g. Langen and Alexeev 2004, Rose *et al* 2013, Eiselt and Graversen 2024), the latitude at which the ocean switches from acting as a heat sink to a heat source, as well as the overall level of ocean heat transport, determines whether the growth of sea ice cover accelerates into the lower latitudes or stays restricted to the polar regions. For our simulations, we found that the semi-idealised $4\times CO_2$ annual-mean q-flux was suitable for sustaining stable polar ice caps.

The surface albedo and shortwave fluxes are computed using the Delta Eddington multiple scattering radiative transfer scheme (Briegleb and Light 2007). In this formulation, the surface albedo is typically adjusted by toggling parameters which control the albedo of bare ice (R_{ice}) or the snow grain radius (R_{snw}), which increases the albedo of snow for decreasing grain radius. Consistent with the study of Kay *et al* (2022), which aimed to improve the simulation of historical Arctic sea ice trends in CESM2 using these types of albedo tuning parameters, we find that small modification of the R_{snw} parameter has outsized effects compared to other tuning parameters and so use it to tune our simulations. After exhaustively investigating the parameter space, we found that an R_{snw} value of 0.7 facilitates the presence of stable polar ice caps. To put this into context, a R_{snw} value of 0.7 produces a dry snow grain radius of 325 μm and a lower albedo than the default value of $R_{snw} = 1.25$ which produces a dry snow grain radius of 187.5 μm. If the default CESM2 R_{snw} value is used the sea ice cover expands too far equatorward and the globe becomes nearly ice-covered.

Compared to the EBM used in EEW22, our model configuration represents a more realistic and comprehensive representation of the climate system and includes important processes such as moisture, cloud physics, snow cover on sea ice, a full three-dimensional representation of the atmosphere, and explicit simulation of the atmospheric circulation. As a numerical testbed for investigating the spurious response to a ghost flux forcing, we have chosen a model configuration which has important idealisations relative to the comprehensive Earth systems models with the most important simplifications being a lack of interactive ocean dynamics, with climatological ocean heat transport being prescribed through the q-flux profile, the lack of land surface, and a lack of sea ice dynamics. We suggest that this choice of model complexity signifies a good compromise between representing the processes which may mediate the zonal-mean response to sea ice loss and directly simulating variables of interest, whilst limiting the computational requirements needed for running a large number of simulations and avoiding the need for very long integrations. The extensive tuning simulations that were completed would have been intractable with the inclusion of the fully dynamic ocean model.

What is the motivation behind the choice of implementing the zero-layer sea ice thermodynamic model rather than a more complex version? Firstly, sea ice dynamics is disabled because we believe this is essentially a thermodynamics problem and so neglecting ice dynamics makes the results easier to understand and interpret. Secondly, our choice of the sea ice representation provides a clear through line back to the study of EEW22 which had a similar setup. In our model configuration, sea ice can influence climate largely through two ways: surface albedo and insulation effects. This is another factor in common with EEW22, however the idealisation that sea ice insulation plays no role in the annual mean response to sea ice loss does not hold in our model because the surface energy budget is not linearly dependent on the surface temperature. Chung and Feldl (2024) investigate the effects of sea ice albedo and insulation in an idealised modelling framework (the ISCA model) with thermodynamic sea ice and compare to the effects of CO_2 and water vapour, and find that the annual mean response to sea ice thinning is very small in that framework. Our simulations utilize a slab ocean and so do not include the freshening effects of sea ice loss and any potential changes in the ocean circulation (e.g. Sevellec *et al* 2017, Li *et al* 2021). Overall, we suggest that this slab ocean aquaplanet configuration of CESM2 coupled to an idealized representation of thermodynamic sea ice is the ideal complexity step in the model hierarchy (Polvani *et al* 2017) to investigate the spurious climate response in sea ice loss simulations and propose a framework which can account for these spurious effects and be applied to comprehensive climate models.

In addition to simulations coupled to the active thermodynamic sea ice model, we also utilize the prescribed ice configuration available in the CICE model (Bailey *et al* 2018). In the default prescribed ice configuration, the sea ice concentration is prescribed to a desired state at each grid cell, the thickness is set to 2 m in the Northern Hemisphere and 1 m in the Southern hemisphere, and the surface fluxes, albedo and surface temperature are calculated. We have modified the CICE prescribed ice module code to also prescribe the sea ice thickness, in addition to sea ice concentration, to a desired state at each grid cell. A similar

approach was taken in Cvijanovic and Caldeira (2015). Thus, the prescribed ice configuration is used to specify the sea ice concentration and thickness monthly-varying climatology from our active sea ice simulations. The prescribed ice simulations have some important differences with the active ice simulations. Firstly, the prescribed ice mode does not conserve energy. Second, there are substantial differences in the simulated seasonal cycle, with the largest differences in the summer, however it is important to note that differences in the simulated annual mean climate are relatively small. Finally, the active sea ice simulations will feature more internal variability than the corresponding prescribed ice simulations in which the only ice related temporal variability is the repeating seasonal cycle around the average state. This suppressed variability could influence the interpretation of our results if the variability rectifies on the average climate response. So as to avoid these potential issues from the differences between the active and prescribed ice modes, we only compare the climate responses solely in either active or prescribed ice modes.

3. Estimating the effects of sea ice loss using the ghost flux method in CESM2 aquaplanet

3.1. Experiments

We first note all experiments in this study are summarised in table 1. We conduct a $1 \times CO_2$ control simulation (CTRL) with a pre-industrial CO_2 mixing ratio of 284.7 ppmv and active sea ice. The CTRL annual average sea ice area is 56.9 $\times 10^6$ km^2 with a seasonal cycle ranging from a maximum of 74.7 $\times 10^6$ km^2 in the late winter to a minimum of 37.6 $\times 10^6$ km^2 in the late summer (figure 1(a)). Compared to the real climate system the sea ice edge is further equatorward by 13° and the seasonal cycle amplitude is 20% too large from the perspective of the migration of the sea ice edge. The CTRL annual average sea ice volume is 254 $\times 10^3$ km^3 with a seasonal cycle amplitude of 25 $\times 10^3$ km^3 (figure 1(b)). We note that, because of the symmetry between the hemispheres in our aquaplanet configuration, metrics for the sea ice are averaged over both poles after aligning the seasonal cycles. In essence, this provides twice the number of years of simulation data, reducing the role for internal climate variability.

The CTRL simulation is paired with a future simulation (FUT) which is identical to CTRL except with a 15% increase in the CO_2 mixing ratio, with a value of 327.4 ppmv. The FUT annual average sea ice area is 37.6 $\times 10^6$ km^2 with a seasonal cycle ranging from a maximum of 56.2 $\times 10^6$ km^2 in the late winter to a minimum of 16.8 $\times 10^6$ km^2 in the late summer (figure 1(a)). This represents an annual mean loss of sea ice of 19.3 $\times 10^6$ km^2 relative to CTRL. The FUT annual average sea ice volume is 57 $\times 10^3$ km^3, a loss of 197 $\times 10^3$ km^3 relative to CTRL. Between FUT and CTRL, the annual mean sea ice edge retreats 11° polewards and the thick sea ice at the very high latitudes undergoes substantial thinning by 3–4 m. The difference between FUT and CTRL is the total climate response to the 15% increase in CO_2 and will contain the role of sea ice loss, as well as other non-ice related factors.

The relatively small increase in CO_2 was chosen so as to simulate a substantial loss of polar sea ice while preserving some sea ice cover in the summer. The climate sensitivity to increasing CO_2 when sea ice is present in this model configuration is surprisingly high. It is unclear whether this sensitivity relates to our choice to use the CESM2 model, or pertains to the slab ocean aquaplanet configuration with thermodynamic sea ice. We note that substituting the idealized zero layer thermodynamic ice model for the more realistic six layer default configuration with mushy layer physics (Bailey *et al* 2018) does not lead to a substantial reduction in the sensitivity. However, we still believe the model configuration is a valuable resource for understanding the spurious climate impacts of sea ice loss intervention and how to correct for it, although this has implications for interpreting the results of this study as discussed in section 5.

In this study, we choose to implement the ghost flux method (Deser *et al* 2015, England *et al* 2020) to perturb the sea ice cover without changing CO_2 using a standard previous methodology to estimate of the role of sea ice loss. We note that the ghost flux method has substantial overlap with the flux nudging approach (McCusker *et al* 2017, Sun *et al* 2018), in which the heat needed to melt the target amount of sea ice is calculated at each time step and applied to the top or bottom of the sea ice component, and as such the results will broadly apply to that method too. The ghost flux simulation (GF) is identical to CTRL except that a constant longwave flux of 10 Wm^{-2} is applied to select areas of sea ice in order to melt the ice. The difference between GF and CTRL is a standard estimate of the climate response to sea ice loss using the ghost flux method.

In GF, the ghost flux is applied in gridboxes, if ice is currently present, in latitudes which experience a monthly zonal mean loss of sea ice concentration of greater than 15% in FUT compared to CTRL. Figure 1(c) shows the seasonally and latitudinally varying, zonally symmetric mask for the ghost flux. This combination of 10 Wm^{-2} and a 15% cutoff was determined iteratively after performing numerous simulations so as to best match the seasonal cycle of sea ice area in GF (figure 1(a), yellow) and FUT (figure 1(a), red). We find that the longwave flux required to melt the sea ice cover in our model setup is much smaller than that used in previous studies: approximately an order of magnitude less than the

Table 1. Table of CESM2 aquaplanet experiments.

Experiment	Name	Forcing	Sea ice	Notes
Control	*CTRL*	$1 \times CO_2$	Active	
Future	*FUT*	$1.15 \times CO_2$	Active	
Ghost flux	*GF*	$1 \times CO_2$	Active	10 W m^{-2} ghost flux applied to ice to match *FUT* ice
Control, FixIce	*CTRL_PI*	$1 \times CO_2$	Prescribed	Sea ice prescribed from *CTRL*
Future, FixIce	*FUT_PI*	$1.15 \times CO_2$	Prescribed	Sea ice prescribed from *CTRL*
Ghost flux, FixIce	*GF_PI*	$1 \times CO_2$	Prescribed	Sea ice prescribed from *CTRL*, ghost flux from *GF* applied to ice

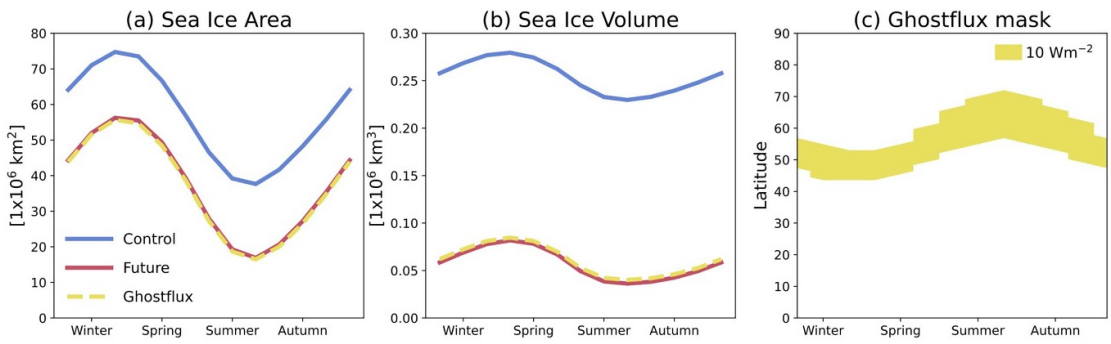

Figure 1. Seasonal cycle of hemispheric average (a) sea ice area and (b) sea ice volume for CTRL (blue solid line), FUT (red solid line) and GF (yellow dashed line) simulations. The seasonal and latitudinal mask over which the 10 Wm^{-2} is applied in GF is shown in panel (c).

seasonally varying flux ranging between 48 Wm^{-2} and 184 Wm^{-2} applied in Deser *et al* (2015). This underscores that the climate in this configuration of CESM2 is more sensitive to external forcing. We also note that, in addition to replicating the FUT sea ice area as designed, the seasonal cycle of sea ice volume in the GF simulation (figure 1(b), yellow) also matches closely to that in FUT (figure 1(b), red). Therefore, the GF simulation is able to replicate the targeted loss of sea ice, both from a seasonal, spatial and thickness perspective, but requires a smaller longwave flux compared to other comprehensive model studies.

Our CTRL, FUT and GF simulations, which are analogous to those performed in previous studies with comprehensive models (e.g. Deser *et al* 2015, England *et al* 2020), are each run for 150 years. The GF simulation is branched from year 150 of CTRL. We average each simulation over the last 100 years, once the sea ice cover in each hemisphere is relatively stable and the ten-year running mean of the top of atmosphere radiative imbalance is below 0.15 Wm^{-2}. We note that even once the simulated climate is in quasi-equilibrium, there remains substantial multi-decadal climate variability, with the annual mean sea ice edge varying by over 4° in each hemisphere in CTRL over the century.

3.2. Nearly all of climate response attributed to sea ice loss according to ghost flux method

We will first discuss the total climate response to an increase in CO_2 in the CESM2 aquaplanet with thermodynamic sea ice, as shown by the left column in figure 2. We note that we focus on the annual mean, zonal mean climate response throughout this study. In response to an increase in CO_2 of 15% our model simulates a global mean surface warming of 5.35 K, with warming amplified in the polar regions (60°–90°) relative to the global mean by a factor of 2.8 (figure 2(a)). This polar amplification is surface dominated, dwarfing the tropical upper tropospheric warming signal (figure 2(c)). There is a substantial weakening of the poleward flank of the midlatitude tropospheric jet (figure 2(e)), consistent with the results of Shaw Smith (2022). In this model configuration the polar influence on the midlatitude jet appears to dominate over the tropical influence (Shaw *et al* 2016, Zappa and Shepherd 2017). In addition there is an increase in precipitation in the midlatitudes and the deep tropics (figure 2(g), blue), with increased evaporation substantially offsetting the precipitation increase in the midlatitudes (figure 2(g), green) and a moderate increase in evaporation in the subtropics leading to a net drying in this region (figure 2(g), black). This hydrological response is consistent with previous slab ocean aquaplanet studies (Feldl *et al* 2017, Bui and Maloney 2020, Russotto and Biasutti 2020, Shaw and Smith 2022). This is coupled with a strengthening of the ascending branch and a weakening of the descending branch of the Hadley circulation (figure 2(i)), consistent with the study of Kim *et al* (2022).

Now, we move on to comparing the total climate response (left column in figure 2) with the estimated climate response to sea ice loss (right column in figure 2). As is clearly evident from the similarity between

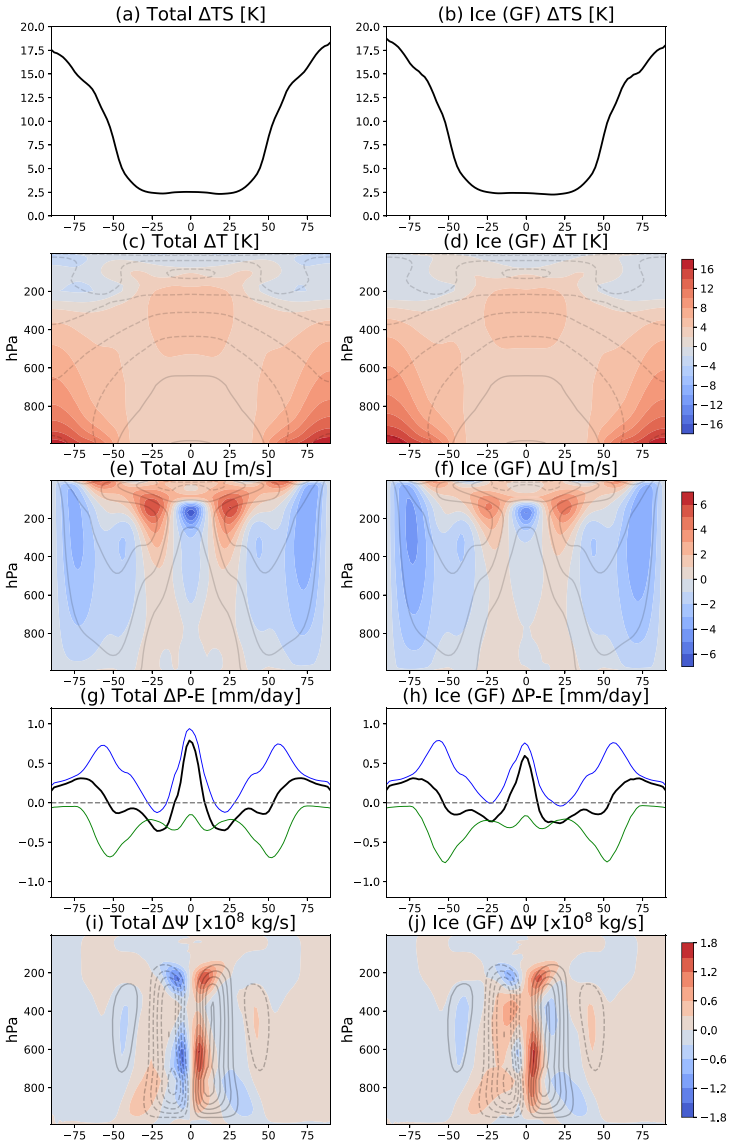

Figure 2. Comparing the full climate response (left column) and estimated role of sea ice loss using the ghost flux method (right column) across a range of annual mean zonal mean climate variables: (a) the surface temperature response, (b) the latitude-height structure of the atmospheric temperature response, (c) the latitude-height structure of the zonal wind response, (d) the precipitation(blue), evaporation (green) and precipitation minus evaporation (black) response, and (e) the latitude-height structure of the meridional streamfunction response. The grey lines indicate the climatology of the CTRL climate in panels (c)–(d), (e)–(f) and (i)–(j) with contour intervals of 20 K, 10 m s^{-1}, and 0.3 × 10^8 kg s^{-1} respectively, with dashed grey lines indicating negative values.

the full climate response and the estimated role of sea ice loss (according to the ghost flux method), this approach suggests that sea ice loss is responsible for nearly all of the surface warming (figure 2(b)), both in magnitude and latitudinal structure, as well as the surface amplified polar warming and tropical upper tropospheric warming (figure 2(d)), the weakening of the poleward flank of the midlatitude tropospheric jet (figure 2(f)), the increase in precipitation in the midlatitudes and in the deep tropics (figure 2(h), blue), the increase in evaporation in the midlatitudes and lower latitudes (figure 2(h), green) and the intensification of the ascending branch of Hadley circulation in the Northern Hemisphere despite an overall decrease in its strength (figure 2(j)). In short, sea ice loss is estimated to be responsible for practically all aspects of the total climate response to increased CO_2 documented in this study, leaving essentially no role for any non-ice related processes. Given that non-ice factors will contribute to all aspects of the climate response, this result is not plausible and highlights the limitations of using the ghost flux method to accurately estimate the role sea ice loss plays under an increase in CO_2.

Although in our aquaplanet experiments the total climate response is approximately identical to the estimated climate response to sea ice loss, we note that this is not a feature found in studies with comprehensive climate model simulations using the ghost flux method (Deser *et al* 2015, Oudar *et al* 2017,

England *et al* 2020, Ringgaard *et al* 2020). However, in these studies nearly all of the high latitude surface warming is attributed to sea ice loss (e.g. Deser *et al* 2015), and in the case of England *et al* (2020) sea ice loss accounts for *more* than 100% of the simulated polar surface warming. Again this raises questions about the ghost flux method because the surface warming response should be polar amplified even in the absence of sea ice loss (England and Feldl 2024), so should certainly not feature near-zero surface warming at the high latitudes. We suggest that differences in the estimated role of sea ice loss outside of high latitudes between our study and previous studies is potentially due to the lack of a dynamical ocean in our model configuration to mediate the climate response to high latitude heating, and to a lesser extent the lack of land. Whatever the case may be, it is easy to see that there is a spurious climate response being erroneously attributed to sea ice loss in our CESM2 aquaplanet experiments. In the next section, we propose a framework for systematically removing the effects of model intervention to provide an estimate of the true role of sea ice loss, and discuss the results of this framework as applied to the CESM2 aquaplanet.

4. Framework for removing the spurious response to model intervention

4.1. Experiments

The overarching idea behind this framework is that the estimate for the climate response to sea ice loss using the ghost flux method includes the actual role of sea ice loss and a spurious contribution arising from artificially applying heat (EEW22). Under the assumption that these different components are additive, the aim here is to isolate the spurious contribution so that it can be subtracted from the ghost flux estimate of the role of sea ice loss to reveal the true role of sea ice loss. Thus, the task is to calculate the effect of the ghost flux intervention absent any changes in sea ice cover. To accomplish this, we perform two simulations with prescribed sea ice concentration and thickness (section 2).

The first, CTRL_PI, is identical to CTRL with the only difference being that the active sea ice is replaced with prescribed ice cover taken from the climatology from years 51–150 of CTRL. Hence, in terms of the long term average sea ice area and volume perspective, these runs have the same sea ice cover, however the sea ice cover in CTRL has temporal variability beyond the seasonal cycle. In the annual mean, the difference between the simulated climates of CTRL and CTRL_PI is relatively small. The largest differences are present in the seasonal cycle, with the CTRL_PI simulation having a cold bias in late winter and a warm bias in late summer in the polar regions, as well as a warm bias near the climatological sea ice edge (figure S1). As in section 3.1, this and the following simulations are each run for 150 years with the climate state averaged over the last 100 years.

The second, GF_PI, is identical to CTRL_PI except that the longwave flux applied in the GF simulation is also applied to the prescribed sea ice cover. This will influence the overlying atmosphere through the surface flux calculation but will not melt the ice. For this purpose, the longwave flux added to each grid cell at each timestep in GF was output and saved as a new variable. Without directly saving this flux, it would be possible to estimate the applied flux from the evolution of the sea ice cover and the ghost flux mask. The difference between GF_PI and CTRL_PI is the spurious climate response to the imposed ghost flux: by design the sea ice cover is unchanged and so there is no contribution from sea ice loss. To isolate our estimate for the true role of sea ice loss, we then subtract this spurious climate response from the estimated climate response to sea ice loss according to the ghost flux method. In terms of our experiments, the true role of sea ice loss is estimated as (GF—CTRL) – (GF_PI—CTRL_PI).

To test the assumption of additivity, we perform an additional prescribed ice simulation, FUT_PI, which is identical to CTRL_PI except that the CO_2 forcing is taken from FUT. Importantly, the prescribed sea ice cover is identical in CTRL_PI and FUT_PI. Therefore, the difference between FUT_PI and CTRL_PI provides an estimate of the climate response to increased CO_2 without the effects of sea ice loss. If the assumption of additivity holds, the response to CO_2 absent sea ice loss and the response to sea ice loss absent the spurious impacts of model intervention should sum to reproduce the total climate response. We will return to discuss this in section 4.4.

4.2. A corrected estimate for the role of sea ice loss in CESM2 aquaplanet

Using our framework, we now turn to removing the spurious climate response from the ghost flux estimate for the role of sea ice loss in the CESM2 aquaplanet. We start with the annual mean zonal mean surface climate response (figure 3). We find that the spurious warming attributed to the ghost flux intervention accounts for 10%–20% of the total surface warming at each latitude band (orange, figures 3(a) and (b)). Therefore removing this artificially induced surface warming reduces the estimated role of sea ice loss from approximately 100% (yellow, figures 3(a) and (b)) to 80%–90% (purple, figures 3(a) and (b)) of the total surface warming, depending on the latitude. Using our framework, we find very similar results for precipitation (figures 3(c) and (d) and evaporation (figures 3(e) and (f)). The spurious contribution to the

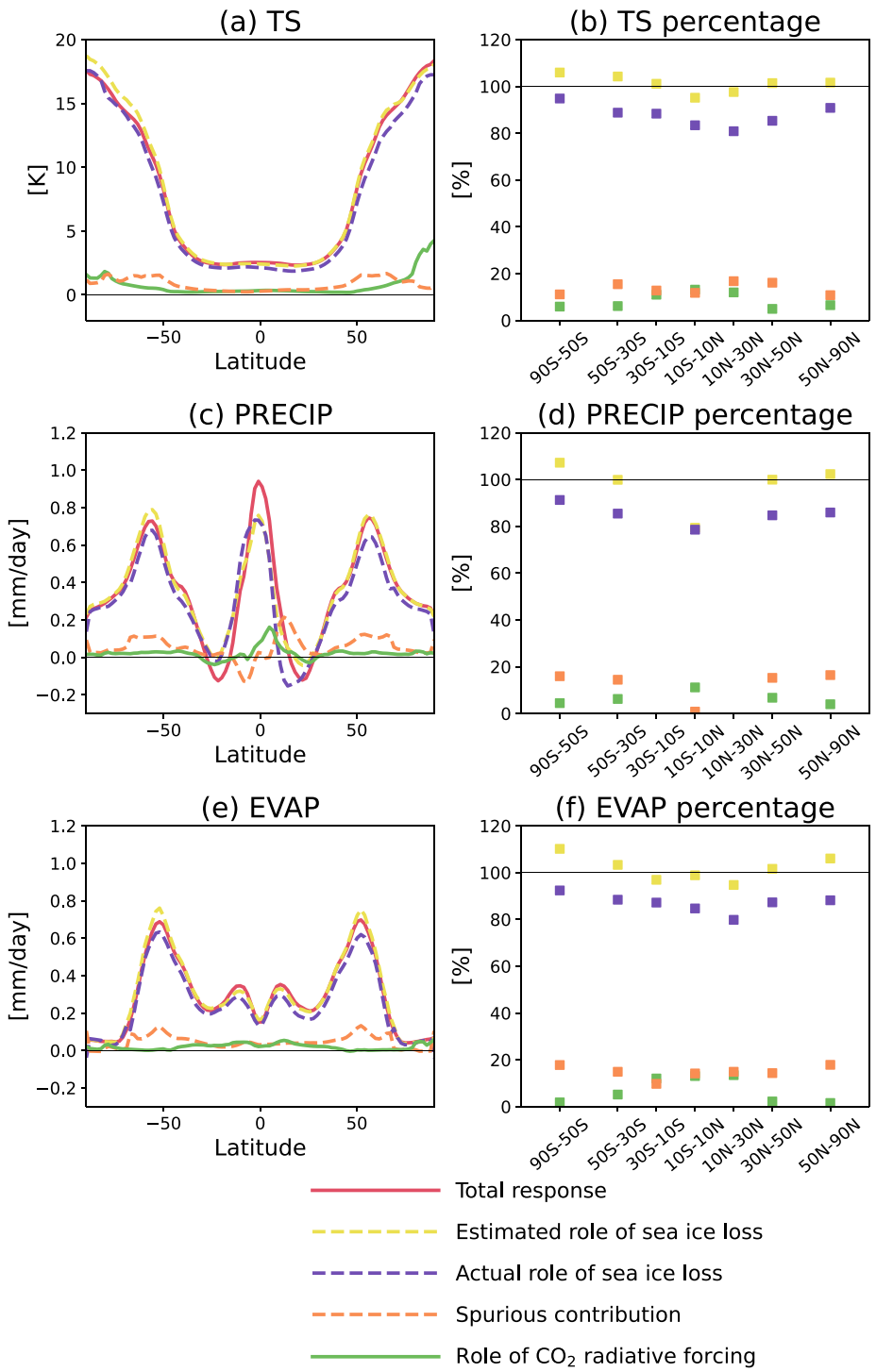

Figure 3. Comparing the total response (solid red line), the ghost flux estimate for the role of sea ice loss (dashed yellow line), the actual role of sea ice loss (dashed purple line), the spurious contribution from the model intervention (dashed orange line) and the role of CO_2 radiative forcing (solid green line), as estimated from our new framework, as applied to the annual mean zonal mean (a) surface temperature response, (c) precipitation response and (e) evaporation response. In panels (b), (d) and (f) we calculate by latitude band the percentage contribution to the total response by the ghost flux estimate for the role of sea ice loss, the actual role of sea ice loss, the spurious contribution from the model intervention and the role of CO_2 radiative forcing, for the annual mean surface temperature, precipitation, and evaporation response respectively.

precipitation response is found to peak slightly off the equator (orange, figure 3(c)) however it is challenging to know if this is a robust results given that all our experiments are hemispherically symmetric. Regardless, our results indicate that the surface warming and hydrological responses to sea ice loss are consistently overestimated in this model configuration, and we estimate the magnitude of this overestimation to be approximately 10%–20%.

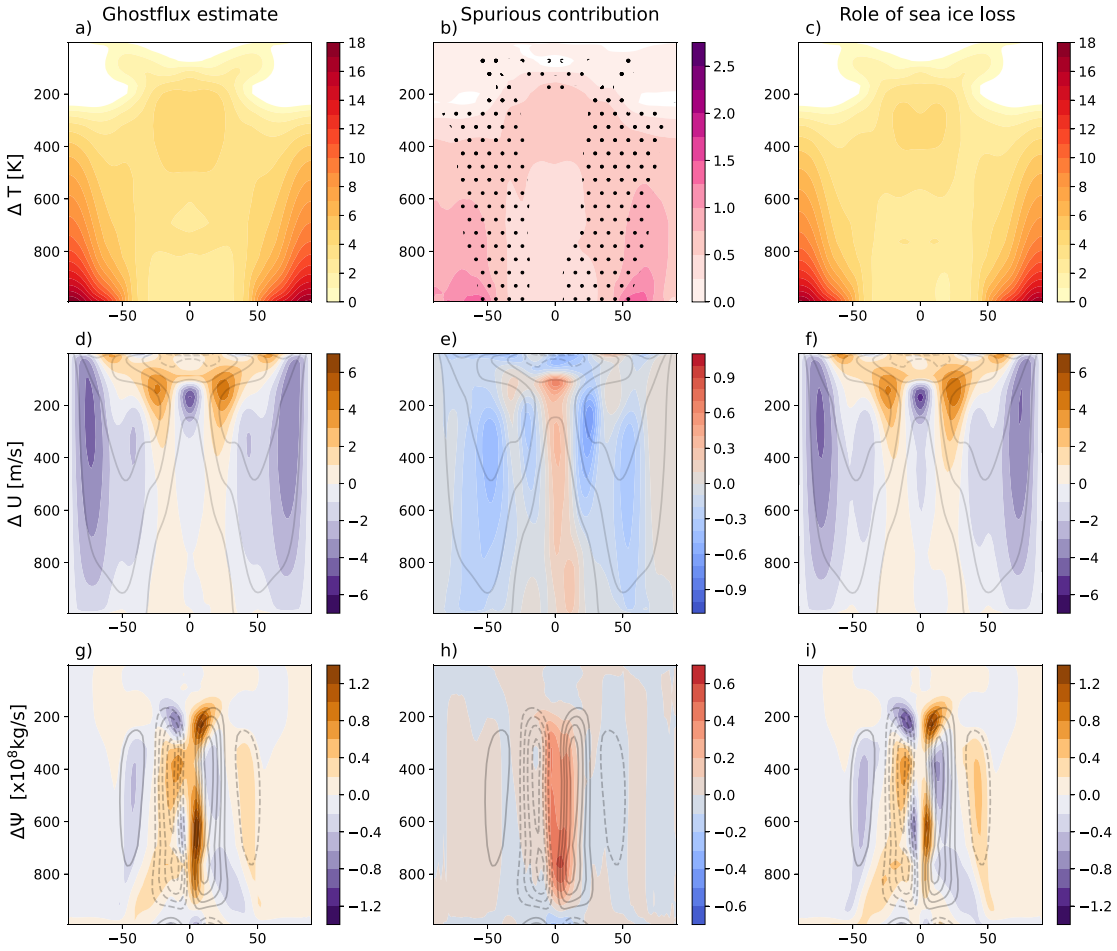

Figure 4. Latitude-height structure of annual-mean zonal mean atmospheric temperature response (top row), zonal wind response (middle row) and streamfunction response (bottom row) for the ghost flux estimate for the role of sea ice loss (left column), the spurious contribution from the ghost flux (centre column) and the true role of sea ice loss (right column). Please note that the middle column has different colour scales than the left and right columns. The dotted area in panel b indicate where the spurious contribution accounts for more than 20% of the ghost flux estimate. The grey contours in the middle row indicate the CTRL climatology of the annual mean zonal mean wind with contour levels of 10 m s^{-1} and the grey contours in the bottom row indicate the CTRL climatology of the annual mean zonal mean streamfunction with contour intervals of 2×10^8 kg s^{-1} where negative values are shown by the grey dashed line.

The breakdown is more nuanced if we look at other metrics of the atmospheric response. For example, in the case of the atmospheric temperature response, while the spurious contribution from the ghost flux intervention (figure 4(b)) is a warming throughout the atmosphere, the spatial structure is distinct from that of the role of sea ice loss (figure 4(c)). The spurious atmospheric warming we identify peaks near the surface around the ice edge, which is consistent with where the ghost flux is applied (figure 1(c)). In essence, this is a relatively localised spurious warming in the proximity of where the artificial heating is applied. In contrast, the actual role of sea ice loss peaks at the poles, not near the sea ice edge.

Why is it important that the spurious contribution from the ghost flux method has this distinct spatial structure? One reason is that it can induce an unexpected circulation response, when considering the zonal wind. One might expect that artificially heating the high latitudes through the ghost flux method would lead to an exaggerated reduction in the equator-to-pole temperature gradient and overestimate the equatorward shift or weakening on the poleward flank of the midlatitude tropospheric jet. Instead, we find that due to the additional localised heating near the sea ice edge, this drives a weakening of the tropospheric jet further equatorward, towards the core and equatorward flank of the tropospheric jet (figure 4(e)). Thus, in our model configuration, the ghost flux method does overestimate the jet response, but on the equatorward flank rather than the poleward flank, (compare figures 4(d) and (f)).

We note that because the CTRL sea ice edge is further equatorward than in other model configurations, as well as in the real world, this could have a different influence on the tropospheric jet. It is possible that our results show a mild overestimate of the effect of sea ice loss on the core and equatorward flank of the tropospheric jet because of the proximity of the ice edge and location of artificial heating to the location of the jet itself. From this perspective, we suggest that the albedo modification method, which adds artificial

heat into the highest latitudes rather than near the CTRL sea ice edge, would drive a robust overestimate of the tropospheric jet response to sea ice loss, specifically on the poleward flank, in line with our original hypothesis rather than an underestimate. This is indeed what Fraser-Leach *et al* (2023) find using the pattern scaling technique, concluding that the weakening of the poleward flank of the winter tropospheric jet is overestimated by 50%. Thus different ice perturbation methods could induce a range of different spurious circulation responses, even if they consistently overestimate the warming response to sea ice loss.

We next examine how the ghost flux method alters the estimated response of the Hadley circulation to sea ice loss. Firstly, it is important to note that projected changes of the strength of the Hadley circulation under climate change have a complex regional structure (Su *et al* 2014, Lau and Kim 2015, Kim *et al* 2022) and vary substantially across models (Su *et al* 2019): most climate models typically suggest an enhancement and narrowing of the Hadley cell's ascending branch (Lau and Kim 2015, Su *et al* 2017), an overall poleward expansion of the Hadley circulation (Lu *et al* 2007, Grise and Davis 2020), with a net weakening of the Northern Hemisphere cell and a net strengthening of the Southern Hemisphere cell (Xia *et al* 2020). Even when considering simulations forced only with an increase in greenhouse gas emissions, the sign of the response of Hadley circulation strength is unclear for the Southern Hemisphere cell (Xia *et al* 2020). In our simulations, in response to sea ice loss as estimated by the ghost flux method, the intensity of the overturning circulation strength as measured by the peak mass flux is largely unchanged. At the pressure level and latitude where the climatological mass flux by the Hadley circulation peaks, sea ice loss is estimated to cause a small weakening of the peak mass flux of 2×10^7 kg s^{-1} approximately cancelling out the contribution from a small strengthening caused by CO_2 absent sea ice loss (not shown). The ascending branch of the Northern Hemisphere Hadley cell intensifies with a weakening of the descending branches in both hemispheres (figure 4(g)): similar to the full response (figure 2(i)) but with a hemispheric asymmetry. Using our framework, this hemispheric asymmetry seems to be a spurious response to the ghost flux intervention (figure 4(h)) despite the ghost forcing being applied without an asymmetry and with all forcings hemispherically symmetric, however internal climate variability will be the ultimate cause. Our corrected estimate of the role of sea ice loss suggests that, in this model configuration, sea ice loss is responsible for most of the weakening of the descending branches of the Hadley circulation (figure 4(i)). Our results suggest that artificially intervening in climate simulations may introduce spurious, unphysical responses, such as the asymmetries in the tropical circulation response, which can be corrected using the framework outlined in our study.

4.3. A surface energy balance interpretation of the spurious response to ghost flux

Next, we attempt to gain insight into precisely how the spurious climate response is caused by the application of the longwave ghost flux. We do this by examining the net surface energy balance for the difference between the GF_PI and CTRL_PI simulations (figure 5). In this figure, red represents a warming impact on the surface and blue represents a cooling.

As expected, the applied longwave ghost flux is evident throughout the area of imposed sea ice loss, peaking in late summer (figure 5(a)). As a reminder to the reader, a longwave flux of 10 W m^{-2} was applied to the base of the sea ice in gridboxes in which sea ice loss occurs under increased CO_2, if sea ice is present at that timestep. As such, 10 W m^{-2} represents an upper bound of what the average forcing would be over the 100 year simulation, because the ice cover would melt in response to the ghost flux as well as fluctuations from natural variability.

Less intuitive is the important role of the shortwave component in inducing the spurious response to the ghost flux, as shown in figure 5(b). This peaks in early summer and is of a larger magnitude than the longwave component (figure 5(a)). In figure S2, we diagnose the main causes of the warming from the shortwave component. We find that in response to the application of the ghost flux, there is an increase in absorbed shortwave at the surface in the absence of clouds (figure S2 dotted black line) which is attributable to a substantial reduction in summer snow cover (figure S2 red line). Put another way, the longwave ghost flux from below will contribute to a melting of the overlying snow. The albedo of dry snow is 0.8–0.9, whereas the albedo of bare ice is lower with a value of 0.5–0.7 (Shine and Henderson-Sellers 1985, Holland *et al* 2021), and so a reduction in snow cover would lead to less incoming shortwave radiation being reflected. We also remind the reader that the snow cover in CESM2 has been found to have important impacts on the simulated climate, as found here and in previous studies (Holland *et al* 2021, Kay *et al* 2022). In our simulations, the shortwave cloud forcing (figure S2 dashed black line) compensates somewhat for the shortwave impact of the reduced snow cover, moderating the net shortwave surface component (figure S2 solid black line) relative to its clear sky counterpart (figure S2 dotted black line). We note that the particulars of the cloud response may be model dependent, however we suggest that the reduction in snow cover as a result of the imposed ghost flux is a robust and physically-based response.

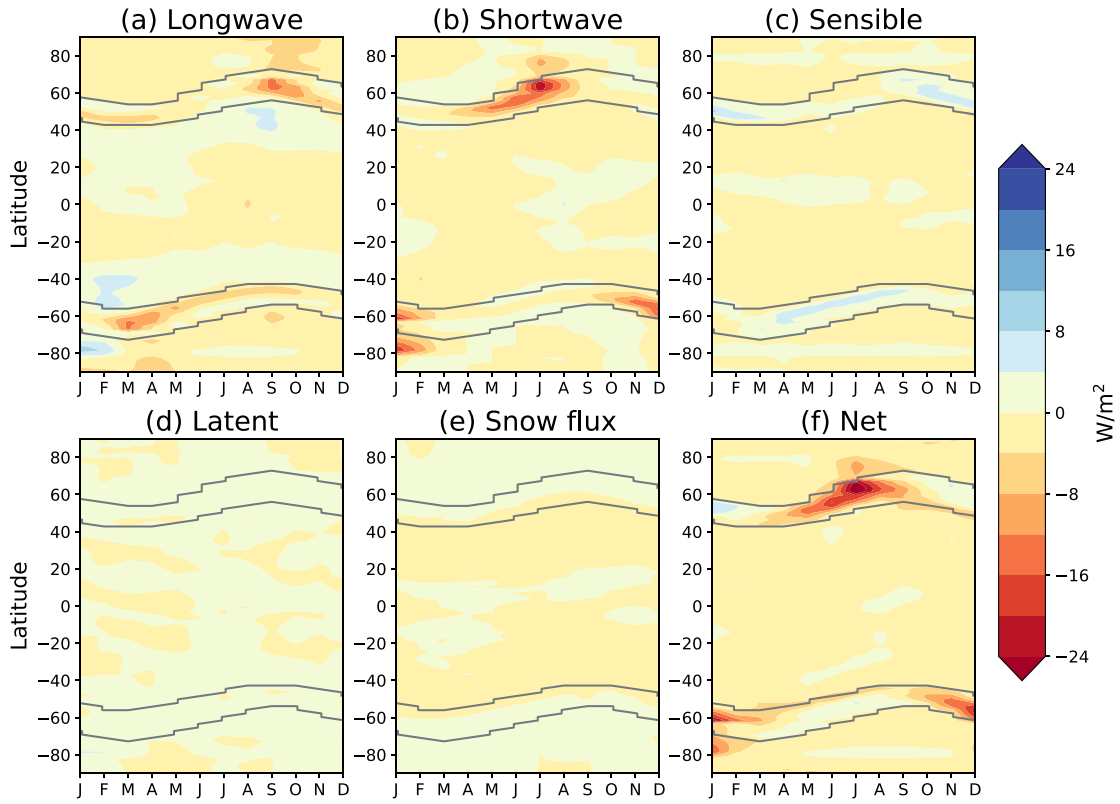

Figure 5. The components of the net surface energy balance for the spurious response to the ghost flux (GF_PI—CTRL_PI): (a) net surface longwave, (b) net surface shortwave (c) sensible heat flux, (d) latent heat flux, (e) snow flux, and (f) the net energy balance. The grey lines show the latitudinal boundaries within which the 10 W m^{-2} ghost flux is applied.

Taken together, our results show that the longwave ghost flux also contributes to the surface warming through a reduction in snow cover and its associated shortwave impacts. Stepping back, we note that while distinctions have been drawn between the various methods for perturbing sea ice cover in coupled simulations, such as through the longwave ghost flux (e.g. Deser *et al* 2015, Oudar *et al* 2017, England *et al* 2020) or via increasing the absorption of shortwave radiation through albedo modification (e.g. Blackport and Kushner 2016, 2017, Sevellec *et al* 2017), the distinction is actually much less clear when looking at their impacts on the coupled system, as shown here by the documented importance of the shortwave feedbacks for the longwave ghost flux forcing.

4.4. Diagnosing the limitations of the new framework

The main assumption at the core of our proposed framework for correcting the estimate for the climate response to sea ice loss is additivity: the true contribution from sea ice loss and the spurious contribution from model intervention are assumed to sum to the ghost flux estimate for the role of sea ice loss, or, equivalently, the true contribution of sea ice loss plus the contribution of non-ice factors should equal the total response. We here test this assumption by analysing whether our estimate for the true response to sea ice loss in the CESM2 aquaplanet sums with an estimate of the response to increased CO_2 radiative forcing to produce the simulated total response. We derive the estimate for the response to CO_2 absent changes in sea ice cover from the difference between FUT_PI and CTRL_PI, which have identical prescribed ice cover but differ in CO_2 forcing.

We present results for the case of the annual mean zonal mean atmospheric temperature response. After subtracting the posited true role of sea ice loss (figure 6(a)) and the estimated role of increased CO_2 (figure 6(c)) from the total climate response, the estimate of the residual temperature response (figure 6(d)) is small throughout much of the atmosphere, suggesting that the responses are approximately separable and additive. The largest residual in the temperature response is at the highest latitudes (figure 6(d)), as is the case with the zonal wind response (figure S3(a)). The residual in the surface temperature response decomposition peaks at the surface (figure S3(c)), which is a region in which our framework attributes too much warming to either sea ice loss or CO_2. The source of this exaggerated warming could be from either the spurious contribution being underestimated in this region, or the contribution from CO_2 being overestimated. While either option is plausible, we suggest that, although modest polar amplification occurs in this model without

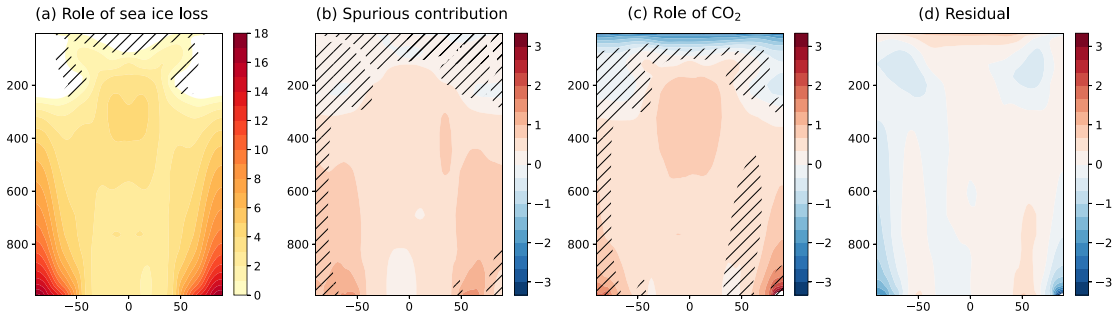

Figure 6. Latitude-height structure of annual-mean zonal mean atmospheric temperature response for the (a) true role of sea ice loss, (b) spurious contribution from the ghost flux, (c) the role of CO_2 radiative forcing, and (d) the residual from the total response after subtracting the role of sea ice loss and the role of CO_2. In panels (a)–(c), the hatching indicates when the magnitude of the estimated response is less than double the magnitude of the residual. As described in the text, here (a) is GF − CTRL − (b), (b) is GF_PI − CTRL_PI, (c) is FUT_PI − CTRL_PI, and (d) is FUT − CTRL − (a) − (c).

sea ice loss (Chung and Feldl 2024, England and Feldl 2024), the substantial localised near-surface warming in response to CO_2 may be unphysical and relate to prescribing the sea ice thickness whilst increasing CO_2. We do note that near the CTRL sea ice edge, where the spurious contribution is identified to peak, the residual is relatively small (see lack of hatching in figure 6(b)). This adds confidence that our framework is performing as intended. The residual for other variables of interest are presented for comparison in figure S3.

In contrast with our framework, the statistical technique for removing the spurious climate response outlined by Fraser-Leach *et al* (2023) does not require any further simulations. However, it cannot be applied to correcting the ghost flux methodology. As such, we suggest further simulations are necessary to estimate the true role of sea ice loss from existing ghost flux simulations. The method we have put forward for removing the spurious effects of model intervention from coupled climate model simulations relies on performing two additional prescribed ice experiments: CTRL_PI and GF_PI. If computational constraints are an issue then a potential alternative solution is to assume that CTRL_PI and CTRL are interchangeable and only perform one additional experiment: GF_PI. When considering the additivity, this approach actually reduces the residual in the atmospheric temperature response (figure S4(d)), in part by reducing the role of CO_2 at the poles near the surface. However, we suggest that there are compensating errors associated with this approach which make the overall error appear small. A new type of error is introduced which involves directly comparing simulations with active sea ice and simulations with prescribed sea ice. These differences are most evident in the seasonal cycle, with the prescribed ice simulations having a larger seasonal cycle, especially near the surface, with the summers being warmer and winters being colder in the high latitudes (figure S1). We note that the impacts on the lower latitudes is small (figure S1(c)). In the annual mean, the CTRL_PI simulation is modestly warmer throughout the atmosphere than in the active ice CTRL simulation (figure S4(e)). Cvijanovic and Caldeira (2015) also report a consistent difference between active and prescribed ice in the an older version of the CESM model, with the prescribed ice simulations similarly being modestly warmer than in the active ice simulation. We remind the reader that in our preferred framework, active sea ice simulations are only directly differenced with other active sea ice simulations and the same for prescribed ice simulations, and so avoid this type of error completely. We have presented estimates of these errors so that modelling groups interested in pursuing this modelling framework can assess their magnitude and understand the tradeoffs which these approaches can introduce.

5. Summary and discussion

In this study we have proposed a new framework for accounting for the spurious climate response inherent to the widely used methods to estimate the effects of sea ice loss in coupled climate model simulations. We apply this framework to the CESM2 aquaplanet, a comprehensive atmospheric model, in which we have coupled a representation of thermodynamic sea ice for the first time. We first replicate the ghost flux method to melt the sea ice cover and obtain a conventional estimate for the climate response to sea ice loss. Our results show that nearly all of the coupled climate response to increased CO_2 is attributed to sea ice loss according to the ghost flux method, which is not physically plausible. We then isolate the true role of sea ice loss in this model configuration by estimating the climate response to the ghost flux absent any changes in sea ice cover and then subtracting this from the ghost flux estimate. The ghost flux method overestimates the surface warming, precipitation and evaporation increase by approximately 10%–20% in this model configuration. There is an important spatial structure to the spurious contribution, with the greatest spurious warming co-located

where the ghost flux was applied. Interestingly, due to this enhanced localised warming, this means that the ghost flux method modestly overestimates the weakening of the midlatitude tropospheric jet in response to sea ice loss, but not on the poleward flank where the largest jet weakening is found. We also find that the ghost flux method spuriously induces an hemispherically asymmetric response of the Hadley circulation. We then elucidate how the ghost flux induces this spurious response: primarily through the longwave imposed flux, and through melting the snow cover overlying the ice, which leads to an increase in the absorption of incoming solar radiation. Lastly, we have identified and quantified the errors associated with this framework.

We find, even after accounting for the spurious effects of model intervention, that sea ice loss influences many far-flung aspects of the climate system: a weakening on the poleward flank of the tropospheric jet, a warming of the tropical upper troposphere, enhanced precipitation in the deep tropics, a net drying of the subtropics, and a weakening of the strength of the Hadley cells outside of the equatorial ascent region. Therefore the response to sea ice loss and the spurious response to ghost flux identified in this study is distinct from the response to sea ice loss and low latitude warming as estimated using the pattern-scaling approach of Hay *et al* (2022) and Hay and Kushner (2024). The statistical-based pattern scaling approach disentangles the role of sea ice loss absent changes in the tropical climate, but we argue that these pathways through low latitude warming are a real part of the response to sea ice loss, although likely overstated in magnitude.

One potential implication from this study could be that the magnitude of the spurious contribution of the ghost flux compared to the true contribution of sea ice loss is relatively small and so can be ignored in comprehensive modelling experiments. We suggest, however, that taking this conclusion from our results would be a mistake. The main reason, beyond wanting to provide as accurate an estimate as possible, is that we believe the magnitude of the spurious influence of the ghost flux diagnosed in this study is a conservative estimate in the context of comprehensive climate model experiments. Why would that be the case? In the CESM2 aquaplanet when thermodynamic sea ice is included, we have found that the climate is extremely sensitive to increases in radiative forcing. We highlight again that we only needed a 15% increase in CO_2 to induce substantial sea ice loss, and the longwave flux needed to melt the sea ice was an order of magnitude less than comparable comprehensive climate model studies. We note that in the absence of sea ice, a quadrupling of CO_2, as compared to a 15% increase, is required to achieve a similar magnitude of global surface warming (England and Feldl 2024). Thus, in this model configuration sea ice loss plays an outsized role relative to both comprehensive climate models and the real world. Given that there is a cap on estimating the role of sea ice loss as 100% of the climate response, it is somewhat inevitable in this model configuration that the spurious contribution will be relatively small. In comprehensive climate model simulations with a dynamic ocean model and a smaller role for sea ice loss in the climate system, this need not be the case. Therefore, while the spurious surface warming and precipitation responses account for 10%–20% of the total climate response to increasing CO_2 in our study, we suggest that this is a conservative estimate and there are robust reasons to believe this fraction will be higher in comprehensive climate model simulations, consistent with the studies of EEW22 and Fraser-Leach *et al* (2023) which estimates that fraction in the range of 30%–50% for the albedo modification method.

In this study we have showcased the use of the framework for isolating the true annual mean climate response to sea ice loss. However, there is substantial interest in exploring the role sea ice loss plays in the midlatitude climate primarily in winter (e.g. Screen *et al* (2018), Smith *et al* (2022)). It remains to be investigated whether our framework can be applied to the climate response in individual months or seasons because the prescribed ice and active ice simulations have different seasonal characteristics. The prescribed ice simulations have an exaggerated seasonal cycle of surface temperature at the high latitudes (figure S1). We note that the pattern scaling approach proposed by Fraser-Leach *et al* (2023) does not have these issues. That being said, the largest differences in our framework are in the summer hemisphere which leaves the potential for the errors in the winter hemisphere to be more tractable. Compounding this, the shortwave cloud forcing response to the ghost flux we found in this study, which may be model dependent, is again confined to the summer.

To conclude, this study provides a framework which other modelling groups can implement to correct existing and planned coupled sea ice loss simulations which rely on the ghost flux or nudging methods for perturbing sea ice cover. In particular, we envisage that this could be a useful resource for the coupled PAMIP simulations (Smith *et al* 2019). This work advances our ability to isolate the true climate response to sea ice loss and leverages the hierarchy of model complexity to link lessons learned from an energy balance model and make them applicable to a state of the art general circulation model.

Data availability statement

Instructions for replicating the configuration of the CESM2 aquaplanet with thermodynamic sea ice is openly available at https://github.com/nfeldl/CESM-icy-aquaplanet. A request has been made to turn this

into a public Component Set Definition for CESM3. The data that support the findings of this study will be openly available following an embargo at the following URL/DOI: https://github.com/nfeldl/CESM-icy-aquaplanet. Data will be available from 31 January 2025.

Acknowledgments

This material is based upon work supported by the National Science Foundation (NSF) under Awards AGS-1753034 and OCE-2048590. MRE is funded by a research fellowship from the Royal Commission for the Exhibition of 1851. Without implying their endorsement, we thank Brian Medeiros, David Bailey, Marika Holland, and Neil Lewis for informative discussions. The aquaplanet model used in this study was made available through the Simpler Models Initiative as part of the Community Earth System Model project; this initiative is supported by the National Center for Atmospheric Research (NCAR) under the sponsorship of the NSF. We acknowledge use of the lux supercomputer at UC Santa Cruz, funded by NSF MRI Grant AST-1828315, and a computing allocation from the CESM Polar Climate Working Group for use of the NCAR supercomputer.

ORCID iDs

M R England https://orcid.org/0000-0003-3882-872X
N Feldl https://orcid.org/0000-0002-2631-1419
I Eisenman https://orcid.org/0000-0003-0190-2869

References

Ayres H, Screen J, Blockley E and Bracegirdle T 2022 The coupled atmosphere–ocean response to Antarctic sea ice loss *J. Clim.* **35** 4665–85

Bailey D, DuVivier A, Holland M, Hunke E, Lipscomb B, Briegleb B, Bitz C and Schramm J 2018 CESM CICE5 users guide *Technical Report* (NCAR)

Blackport R and Kushner P 2016 The transient and equilibrium climate response to rapid summertime sea ice loss in CCSM4 *J. Clim.* **29** 401–17

Blackport R and Kushner P 2017 Isolating the atmospheric circulation response to Arctic sea ice loss in the coupled climate system *J. Clim.* **30** 2163–85

Briegleb B and Light B 2007 A Delta-Eddington multiple scattering parameterization for solar radiation in the sea ice component of the community climate system model *NCAR Technical Note NCAR/TN-472+STR* (National Center for Atmospheric Research) (available at: https://github.com/CICE-Consortium/CICE/blob/master/doc/PDF/BL_NCAR2007.pdf)

Bui H and Maloney E 2020 Changes to the Madden-Julian oscillation in coupled and uncoupled aquaplanet simulations *J. Adv. Model. Earth Syst.* **12** e2020MS002179

Chung P and Feldl N 2024 Sea ice loss, water vapor increases and their interactions with atmospheric energy transport in driving seasonal polar amplification *J. Clim.* **37** 2713–25

Cvijanovic I and Caldeira K 2015 Atmospheric impacts of sea ice decline in CO_2 induced global warming *Clim. Dyn.* **44** 1173–86

Danabasoglu G *et al* 2020 The Community Earth System Model Version 2 (CESM2) *J. Adv. Model. Earth Syst.* **12** e2019MS001916

Deser C, Tomas R and Sun L 2015 The role of ocean-atmosphere coupling in the zonal-mean atmospheric response to Arctic sea ice loss *J. Clim.* **28** 2168–86

Eiselt K and Graversen R 2024 On the impact of net-zero forcing q-flux change *Clim. Dyn.* **62** 4063–79

England M, Eisenman I and Wagner T 2022 Spurious climate impacts in coupled sea ice loss simulations *J. Clim.* **35** 3801–11

England M and Feldl N 2024 Robust polar amplification in ice-free climates relies on ocean heat transport and cloud radiative effects *J. Clim.* **37** 2179–97

England M, Polvani L M and Sun L 2020 Robust Arctic warming caused by Antarctic sea ice loss *Environ. Res. Lett.* **15** 104005

England M, Polvani L, Sun L and Deser C 2020 Tropical climate responses to projected Arctic and Antarctic sea ice loss *Nat. Geosci.* **13** 275–81

Feldl N, Anderson B and Bordoni S 2017 Atmospheric eddies mediate lapse rate feedback and Arctic amplification *J. Clim.* **30** 9213–24

Fraser-Leach K, Kushner P and Audette A 2023 Correcting for artificial heat in coupled sea ice perturbation experiments *Environ. Res.: Climate* **3** 015003

Grise K and Davis S 2020 Hadley cell expansion in CMIP6 models *Atmos. Chem. Phys.* **20** 5249–68

Hay S, Kushner P J, Blackport R, McCusker K E, Oudar T, Sun L, England M, Deser C, Screen J A and Polvani L M 2022 Separating the influences of low-latitude warming and sea ice loss on Northern Hemisphere climate change *J. Clim.* **35** 2327–49

Hay S and Kushner P 2024 The relative importance of Antarctic sea-ice loss within the response to greenhouse warming *J. Clim.* **37** 3323–44

Holland M, Clemens-Sewall D, Landrum L, Light B, Perovich D, Polashenski C, Smith M and Webster M 2021 The influence of snow on sea ice as assessed from simulations of CESM2 *Cryosphere* **15** 4981–98

Kay J *et al* 2022 Less surface sea ice melt in the CESM2 improves Arctic sea ice simulation with minimal non-polar climate impacts *J. Adv. Model. Earth Syst.* **14** e2021MS002679

Kim D, Kim H, Kang S, Stuecker M and Merlis T 2022 Weak Hadley cell intensity changes due to compensating effects of tropical and extratropical radiative forcing *npj Clim. Atmos. Sci.* 61 **5**

Langen P and Alexeev V 2004 Multiple equilibria and asymmetric climates in the CCM3 coupled to an oceanic mixed layer with thermodynamic sea ice *Geophys. Res. Lett.* **31** L04201

Lau W and Kim K 2015 Robust Hadley circulation changes and increasing global dryness due to CO_2 warming from CMIP5 model projections *PNAS* **112** 3630–5

Li H, Fedorov A and Liu W 2021 AMOC stability and diverging response to Arctic sea ice decline in two climate models *J. Clim.* **34** 5443–60
Lu J, Vecchi G and Reichler T 2007 Expansion of the Hadley cell under global warming *Geophys. Res. Lett.* **34** L06805
McCusker K, Kushner P, Fyfe J, Sigmond M, Kharin V and Bitz C 2017 Remarkable separability of circulation response to Arctic sea ice loss and greenhouse gas forcing *Geophys. Res. Lett.* **44** 7955–64
Oudar T, Sanchez-Gomez E, Chauvin F, Cattiaux J, Terray L and Cassou C 2017 Respective roles of direct GHG radiative forcing and induced Arctic sea ice loss on the Northern Hemisphere atmospheric circulation *Clim. Dyn.* **49** 3693–717
Peings Y, Labe Z and Magnusdottir G 2021 Are 100 ensemble members enough to capture the remote atmospheric response to +2 °C Arctic sea ice loss? *J. Clim.* **34** 3751–69
Polvani L, Clement A, Benedict J and Simpson I 2017 When less is more: opening the door to simpler climate models *Eos* **98** 15–16
Ringgaard I, Yang S, Kaas E and Christensen J 2020 Barents-Kara sea ice and European winters in EC-Earth *Clim. Dyn.* **54** 3323–38
Rose B, Ferreira D and Marshall J 2013 The role of oceans and sea ice in abrupt transitions between multiple climate states *J. Clim.* **26** 2862–79
Russotto R and Biasutti M 2020 Polar amplification as an inherent response of a circulating atmosphere: results from the TRACMIP aquaplanets *Geophys. Res. Lett.* **47** e2019GL086771
Screen J, Deser C, Smith D, Zhang X, Blackport R, Kushner P, Oudar T, McCusker K and Sun L 2018 Consistency and discrepancy in the atmospheric response to Arctic sea-ice loss across climate models *Nat. Geosci.* **11** 155–63
Semtner A 1976 A model for the thermodynamic growth of sea ice in numerical investigations of climate *J. Phys. Oceanogr.* **6** 379–89
Sevellec F, Fedorov A and Liu W 2017 Arctic sea-ice decline weakens the Atlantic meridional overturning circulation *Nat. Clim. Change* **7** 604–10
Shaw T *et al* 2016 Storm track processes and the opposing influences of climate change *Nat. Geosci.* **9** 656–64
Shaw T and Smith Z 2022 The midlatitude response to polar sea ice loss: idealized slab-ocean aquaplanet experiments with thermodynamic sea ice *J. Clim.* **35** 2633–49
Shine K and Henderson-Sellers A 1985 The sensitivity of a thermodynamic sea ice model to changes in surface albedo parameterisation *J. Geophys. Res.* **90** 2243–50
Simon A, Gastineau G, Frankignoul C, Rousset C and Codron F 2021 Transient climate response to Arctic sea ice loss with two ice-constraining methods *J. Clim.* **34** 3295–310
Smith D *et al* 2019 The Polar Amplification Model Intercomparison Project (PAMIP) contribution to CMIP6: investigating the causes and consequences of polar amplification *Geosci. Model. Dev.* **12** 1139–64
Smith D *et al* 2022 Robust but weak winter atmospheric circulation response to future Arctic sea ice loss *Nat. Commun.* **13** 727
Su H *et al* 2017 Tightening of tropical ascent and high clouds key to precipitation change in warmer climate *Nat. Commun.* **8** 15771
Su H, Jiang J, Zhai C, Shen T, Neelin J, Stephens G and Yung Y 2014 Weakening and strengthening structures in the Hadley circulation change under global warming and implications for cloud response and climate sensitivity *J. Geophys. Res. Atmos.* **119** 5787–805
Su H, Zhai C, Liang J, Wu L, Neelin J and Yung Y 2019 A dichotomy between model responses of tropical ascent and descent to surface warming *npj Clim. Atmos. Sci.* **2** 8
Sun L, Alexander M and Deser C 2018 Evolution of the global coupled climate response to Arctic sea ice loss during 1990–2090 and its contribution to climate change *J. Clim.* **31** 7823–43
Sun L, Deser C and Alexander M 2020 Global coupled climate response to polar sea ice loss: evaluating the effectiveness of different ice-constraining approaches *Geophys. Res. Lett.* **47** e2019GL085788
Xia Y, Hu Y and Liu J 2020 Comparison of trends in the Hadley circulation between CMIP6 and CMIP5 *Sci. Bull.* **65** 1667–74
Zappa G and Shepherd T 2017 Storylines of atmospheric circulation change for European regional climate impact assessment *J. Clim.* **30** 6561–77
Zhu J, Otto-Bliesner B, Brady E C, Gettelman A, Bacmeister J T, Neale R B, Poulsen C J, Shaw J K, McGraw Z S and Kay J E 2022 LGM paleoclimate constraints inform cloud parameterizations and equilibrium climate sensitivity in CESM2 *J. Adv. Model. Earth Syst.* **14** e2021MS002776